Published in "Biomacromolecules 13(10): 3241–3252, 2012"
which should be cited to refer to this work.

Gelation, Phase Behavior, and Dynamics of β-Lactoglobulin Amyloid Fibrils at Varying Concentrations and Ionic Strengths

Sreenath Bolisetty,[†] Ludger Harnau,[‡] Jin-mi Jung,[§] and Raffaele Mezzenga*[,†]

[†]ETH Zurich, Food and Soft Materials Laboratory, Department of Health Science and Technology, Schmelzbergstrasse 9, LFO-E22, CH-8092 Zurich, Switzerland

[‡]Max-Planck-Institut für Intelligente Systeme, Heisenbergstrasse 3, 70569 Stuttgart, Germany, and Institut für Theoretische und Angewandte Physik, Universität Stuttgart, Pfaffenwaldring 57, 70569 Stuttgart, Germany

[§]Department of Physics, University of Fribourg, Ch. Musée 3, CH-1700 Fribourg, Switzerland

ABSTRACT: We have investigated the thermodynamic and dynamic behavior of multistranded β-lactoglobulin protein fibrils in water, by combining static, dynamic, and depolarized dynamic light scattering (SLS, DLS, DDLS), small angle neutron scattering (SANS), rheology, and cryogenic transmission electron microscopy (cryo-TEM). We focus on the region of the phase diagram at which ionic strength and concentration changes induce transitions in gelation and lyotropic liquid crystalline behavior. An increase in ionic strength, induced by NaCl salt, progressively causes the phase transitions from nematic (N) to gel (G) phases; a further increase causes the transition to a translucent phase and to a macroscopic phase separation, respectively. An increase in fibril concentration induces first a phase transition from an isotropic (I) to a nematic phase (N); a further increase induces the formation of a gel phase. The protein gel strength is investigated by rheology measurements. SANS and osmotic compressibility calculated by SLS measurements clearly capture the main features of the IN transition of β-lactoglobulin protein fibrils. The form and structure factors measured by scattering experiments are analyzed by the polymer reference interaction site model (PRISM). Dynamics of the protein fibrils at different concentrations, measured by polarized and depolarized dynamic light scattering, show both individual and collective diffusion after the isotropic−nematic transition. Above this transition, cryo-TEM images further demonstrate the alignment of the protein fibrils, which is quantified by a 2D order parameter. This work discusses comprehensively, both experimentally and theoretically, the thermodynamics and dynamic features of β-lactoglobulin amyloid fibrils in a vast region of the concentration−ionic strength phase diagram.

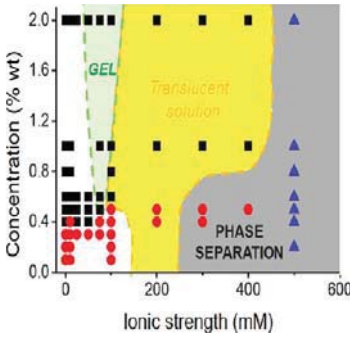

β-lactoglobulin is the major globular whey protein found in bovine milk.[1] The monomer unit of the protein is relatively small having the radius about 2 nm and molar mass of 18.4 kDa. The native protein monomer solutions are stable due to electrostatic repulsions but start to aggregate near the isoelectric point (pI = 5.1).[2] If the temperature or pressure of the protein solution are increased, the protein gets partially denatured and starts to aggregate.[3] The structure[4] and size of the aggregate[5] depend on the protein concentration, pH of the solution,[6] ionic strength, and several other parameters of the heating protocol. When the protein solution concentration is higher than a critical concentration, networking of the aggregates and gel formation are observed.[7] Below this critical concentration, the structure of the soluble aggregates primarily depends on the pH and ionic strength of the solution.[8] For example, wormlike primary aggregates are formed at pH 7.0, spherical aggregates at pH 5.8, and long, semiflexible multistranded amyloid fibrils are formed at low acidic pH conditions, when the ionic strength is low.[4,9] In-depth analysis of the fibril structures and kinetics of formation of these multistranded amyloid fibrils below the gelation concentration threshold has been carried out using atomic force microscopy[10] or a combination of atomic force microscopy and scattering techniques.[11]

Beyond a critical concentration, β-lactoglobulin aggregates into a vast typology of gels. In addition to heat-induced gelation of the β-lactoglobulin protein, the cold set gelation[12,13] has progressively gained increasing attention due to its superior properties[14] such as higher gel strength and fracture properties, improved water-holding capacity, transparency, and fine stranded structure. In traditional cold setting gelation, the protein solutions are first heated and partially unfolded at pH around 7 and subsequently cooled down, and then gelation is induced by mono or multivalent salt solutions[15] such as NaCl, $CaCl_2$. Much higher concentrations of NaCl are required for cold gelation compared to $CaCl_2$ salt solution.[16] The main features and applications of these gels are summarized in the recent literature.[17]

Multistep cold gelation of β-lactoglobulin mature fibrils prepared at low pH, induced by Ca^{2+} salt solutions has been shown by the group of Van der Linden.[18] In their work, the pH of the fibril suspension was adjusted to pH 7, and a multivalent calcium salt solution was subsequently added to induce gel formation. The salt was purposely chosen as multivalent to induce bridging among fibrils at very low concentrations, and indeed at comparable concentrations of NaCl, no gelation was observed.[18] In this manuscript, NaCl salt is selected, and the concentration is varied to achieve the slightly different role of tuning the total ionic strength without electrostatic cross-links among the fibrils; to this end, we deliberately fix the pH fibrils solution at pH 2 and simply induce gelation by varying the Debye length upon increasing the ionic strength. We map the complete phase diagram of fibrils at different NaCl concentrations and protein fibril concentrations and assess the gel strengths by rheology. We focus on the collective behavior of the protein fibrils at different concentrations and ionic strength; the impact of NaCl salt solution on individual β-lactoglobulin fibril structures has been reported in a previous work.[19]

In the second part of the manuscript, we discuss in detail the lyotropic liquid crystalline phase formation of the β-lactoglobulin fibril solutions investigated by both static and dynamic scattering techniques. At sufficiently high concentrations, biopolymer solutions of DNA, peptides, polymer/peptide hybrids can orient to form lyotropic liquid crystalline mesophases due to excluded volume interactions.[20] Amyloid fibrils do follow similar trends and indeed, the mesoscopic phase behavior of concentrated β-lactoglobulin fibril suspensions has also been reported experimentally,[21,22] and rationalized using excluded volume interactions both as a function of pH and ionic strength.[23] Similarly, lysozyme fibrils have also been shown to self-organize into liquid crystalline structures.[24,25]

In this manuscript, we greatly expand the range of concentrations and ionic strengths within which β-lactoglobulin fibril suspensions phases are studied, and we use an unprecedented set of experimental techniques and theoretical descriptions to shed further light into the thermodynamic behavior of this colloidal system. The lyotropic liquid crystalline transition of these fibrils is studied in detail by combining small angle neutron scattering (SANS) with static light scattering (SLS). The static intensities measured at different concentrations of the β-lactoglobulin solutions are successfully fitted with theoretical predictions. Additionally, we study the dynamic behavior of the protein fibril suspensions both at the isotropic−nematic and sol−gel transitions by dynamic light scattering and depolarized dynamic light scattering techniques (DLS, DDLS). While DLS yields the translational diffusion coefficient of any colloidal entity, DDLS is a very sensitive technique to probe anisotropic objects and provides the rotational diffusion of the particles in the suspension.[26] Thus, both the individual and collective translational and rotational diffusion coefficients can be resolved at the isotropic−nematic transition. Finally, we complete the study by quantifying the order in the nematic phase by a two-dimensional orientation order parameter in cryo-transmission electron microscopy (cryo-TEM) images.

EXPERIMENTAL SECTION

Preparation of β-Lactoglobulin Amyloid Fibrils. Bio PURE β-lactoglobulin (lot JE 003-6-922) was obtained from Davisco Foods International, Inc. (Le Sueur, MN) and purified as described in ref 4. In order to produce semiflexible fibrillar aggregates, we followed the same protocol described in ref 4. To optimize contrast of the scattering lengths in the SANS measurements, D_2O was preferred to H_2O: the freeze-dried protein monomer was dissolved in D_2O at a concentration of 2 wt %, pD =2 and the vials were placed in a water bath with temperature maintained constant at 90 °C (±0.1 °C). Different concentrations of the protein fibrils were prepared upon diluting the initial 2 wt % D_2O or H_2O suspensions. The ionic strength was further adjusted to the desired value by using NaCl. These dispersions were then used for mapping the phase diagram and for performing scattering and microscopy experiments.

Small Angle Neutron Scattering Measurements (SANS). SANS measurements were performed at the SANS II facilities of the SINQ Swiss Neutron source at the Paul Scherrer Institute, Switzerland. Quartz cells (1 mm) from Hellma were used. Combinations of different wavelengths (4.55 and 6.37 $Å^{-1}$), sample-to-detector distances (1.2−3 m) and collimation lengths (2−6 m) resulted in an effective q range of 0.1−3 nm^{-1}. The raw spectra were corrected for background from the solvent (D_2O), empty cell and electronic noise using conventional procedures. The two-dimensional isotropic scattering spectra were corrected for detector efficiency according to standard SANS II data reduction procedures, and then neutron scattering intensity vs a scattering vector was obtained by performing radial averages.

Static, Dynamic, and Depolarized Dynamic Light Scattering. The different concentrations of β-lactoglobulin fibrils were also studied by light scattering using a He−Ne laser emitting a polarized light beam of wavelength of 632.8 nm. The simultaneous cross-correlated static and dynamic light scattering measurements were performed at different scattering angles ranging from 40° to 140° at steps of 10° by averaging 3 runs of 600 s each. For depolarized dynamic light scattering measurements, two Glan-Thomson polarizers with extension coefficients higher than 10^{-5} were used in front of the detector to measure the depolarized scattered intensity. In dynamic light scattering, the time correlation function (TCF) of the scattered electric field was analyzed by the CONTIN method, which allows distinguishing individual and collective particles diffusion caused by the nematic ordering of the fibrils.

Rheological Measurements. Rheology measurements were performed using a stress-controlled rheometer (AR2000, TA Instruments) with stainless steel cone and plate geometry (20 mm diameter and angle 2°) at 25 °C with a truncation gap of 59 μm. A solvent trap provided by the manufacturer for liquid samples was used in order to prevent loss of solvent. First, oscillatory stress and strain sweeps were performed to determine the linear viscoelastic region for each sample. Subsequently, the dynamic moduli (G' and G'') were determined using an oscillatory time sweep test for 10 min at a constant strain of 1% and constant frequency of 6.28 rad/s. Frequency sweep experiments were performed at a low amplitude of strain (in linear regime), in the frequency range of 0.1−100 rad/s. The gel strength was quantified by the evaluation of the shear storage modulus G'. To investigate the recovery of the gel after network destruction, viscoelastic properties of gel samples were measured as a function of time in an oscillatory time sweep (5 min, 1% strain, 1 Hz frequency) before and after severe destruction of the gel network (100% strain, 1 min, 1 Hz frequency).

Cryo-Transmission Electron Microscopy. Cryo-TEM measurements of the various concentration of the protein fibril dispersions were carried out on a FEI, model CM12, NL TEM. Sample solutions (2.5 μL) were deposited onto glow-discharged lacey grids, blotted, and frozen in liquid ethane using a Vitrobot plunge freezer. Vitrified specimens were then transferred and mounted under liquid nitrogen onto a cryo-transmission electron microscopy holder and finally transferred to a CM12 TEM maintaining a temperature below −160 °C during transfer and imaging. Frozen hydrated fibril solutions were recorded under low-dose conditions at 100 kV. Electron micrographs were digitally recorded using a Gatan 794 CCD camera.

RESULTS AND DISCUSSION

β-Lactoglobulin protein monomers undergo the formation of mature amyloid fibril structures at pH 2 after the heat treatment of 5 h and temperature of 90 °C.[4] A representative AFM image of the mature multistranded protein fibrils is shown in the Supporting Information, Figure S1. It shows the typical semiflexible protein β-lactoglobulin fibrils, polydispersed in length and with an average cross-section ranging from 2 to 8 nm. The persistence length of these as prepared-β-lactoglobulin amyloid fibrils is approximately an integer multiple n of ~1000 nm where the integer n indicates the number of protofilaments forming the fibrils.[10,27] The mechanism for the formation of mature fibrils from the single protofilaments has been already discussed in detail in our earlier reports.[10,11]

The protein fibrils dispersion is isotropic in nature at diluted-enough conditions. With increasing the protein concentration above a certain critical concentration, fibrils undergo orientation along a common nematic director. The driving force toward orientation is due to excluded volume interactions and to the gain in the free volume entropy and bears some similarity with the entropy-driven crystallization of monodisperse colloidal particles.[27] The isotropic–nematic transition depends on protein fibril concentration, pH, and ionic strength of the solution and can be correctly interpreted and predicted by the Onsager theory considering charge double layers effects, as discussed by Mezzenga et al.[23]

Figure 1 shows the complete phase diagram of β-lactoglobulin amyloid fibrils at various fibril concentrations and ionic strengths and with constant temperature and pH (20 °C, pH = 2). In a previous work we have mapped a much narrower region of the phase diagram up to 1 wt % protein fibril concentration and 100 mM ionic strength.[23] Here, we explore a much wider region of the phase diagram, with concentrations up to 2 wt % and ionic strength up to 600 mM. Interestingly, we found the existence of an intermediate gel phase centered at ionic strength around 100 mM and for concentrations beyond 0.5 wt %. The phase transition from isotropic to nematic phase is observed visually under polarized light. The solutions were transparent, and no birefringence was observed under cross-polarized light until below 0.4 wt % of protein fibril solutions. From 0.4 wt %, the solution starts to exhibit birefringence, revealing the appearance of a nematic phase, in agreement with our earlier observations.[22,23] Increase in the ionic strength from 200 mM onward changes the solution appearance from transparent to translucent. Further, increase in ionic strength causes the phase separation of the solution. The increase in ionic strength induces the screening of the electrostatic interactions. This has a number of consequences on the colloidal dispersion. First, at the single fibril structural level, the increase in ionic strength leads to a progressive untwist of the fibrils, as the electrostatic driving force to twisting is reduced, as discussed in our earlier work both experimentally and theoretically.[19] Then, excluded volume interactions inclusive of the electronic double layer are also decreased. For a fixed concentration, this leads first to a delay in the isotropic–nematic transition, as observed in Figure 1 and as discussed in detail earlier.[23] Finally, with the screening of the electrostatic repulsive interactions, the hydrophobic and van der Waals attractive interactions start to take progressively over, inducing the formation of a gel, based on interfibrillar physical contacts.

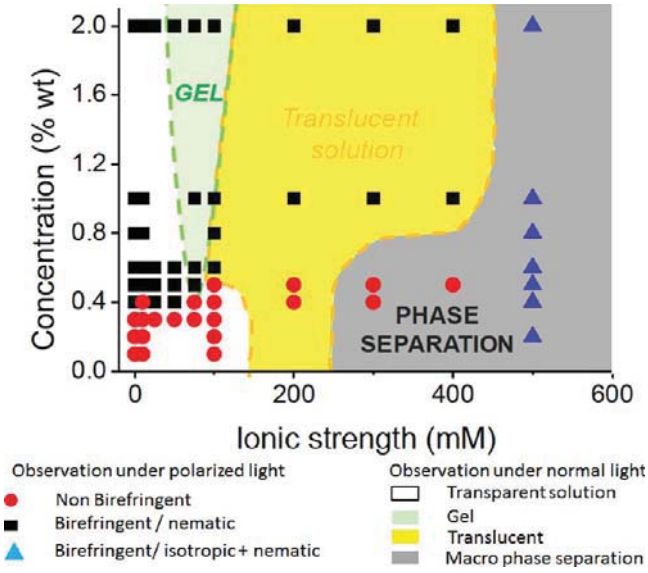

Figure 1. Phase diagram of the β-lactoglobulin amyloid fibrils in water at different concentrations of protein fibrils and different ionic strengths.

The strength of the gel formed at 2 wt % β-lactoglobulin amyloid fibrils as a function of the different ionic strengths is characterized by rheology measurements. Representative frequency sweep tests are shown in Figure 2. The storage modulus (G') is represented by filled symbols, and the loss modulus (G'') is indicated by open symbols in Figure 2A–C. With the increase in ionic strength from 0 mM to the 50 mM, the formation of the gel is revealed by the storage modulus, which is at least 1 order of magnitude larger than the loss modulus over the entire frequency range (Figure 2A). The upturn in the storage modulus G' at high frequency is expected based on rheometer inertia effects at high frequency. Further, an increase in ionic strength from 50 mM to 100 mM causes a further increase in the gel strength, with storage modulus raising from 19.3 to 35.6 Pa at a frequency of 1 rad/s. Additional increase of the ionic strength to 200 mM, leads to a decrease in the strength of the gel. The frequency sweeps measurement at 200 mM ionic strength in Figure 2C shows that storage modulus is now lower than the loss modulus and that the storage modulus at 200 mM ionic strength is lower than that at 100 mM ionic strength. This is due to the onset of macroscopic aggregation of fibrils, as shown in the phase diagram of Figure 1, which leads to a degradation of the gel physical properties. To quantify this effect, the storage modulus at the different salt concentrations is plotted against frequency in Figure 2D. It clearly shows that with the increase in ionic strength from 0 mM to 50 mM and 100 mM, the storage modulus increases gradually, while on a further increase in ionic strength to 200 mM and 400 mM, it gradually decreases.

In addition, we also investigated the self-healing behavior of the gels, after complete structural destruction. Self-healing or gel recovery behavior of the gels is an additional desirable feature of some physical gels, opening for potential applications in biotechnology. In order investigate this effect, 100% oscillatory shear rate was applied to a preformed gels prepared at a concentration of 2 wt % protein fibrils and ionic strength of 50 mM. High shear amplitudes completely destruct the gel, which immediately after rupture shows the typical liquid behavior. The restoration of the storage modulus, representative of structural recovery, was then monitored over time.

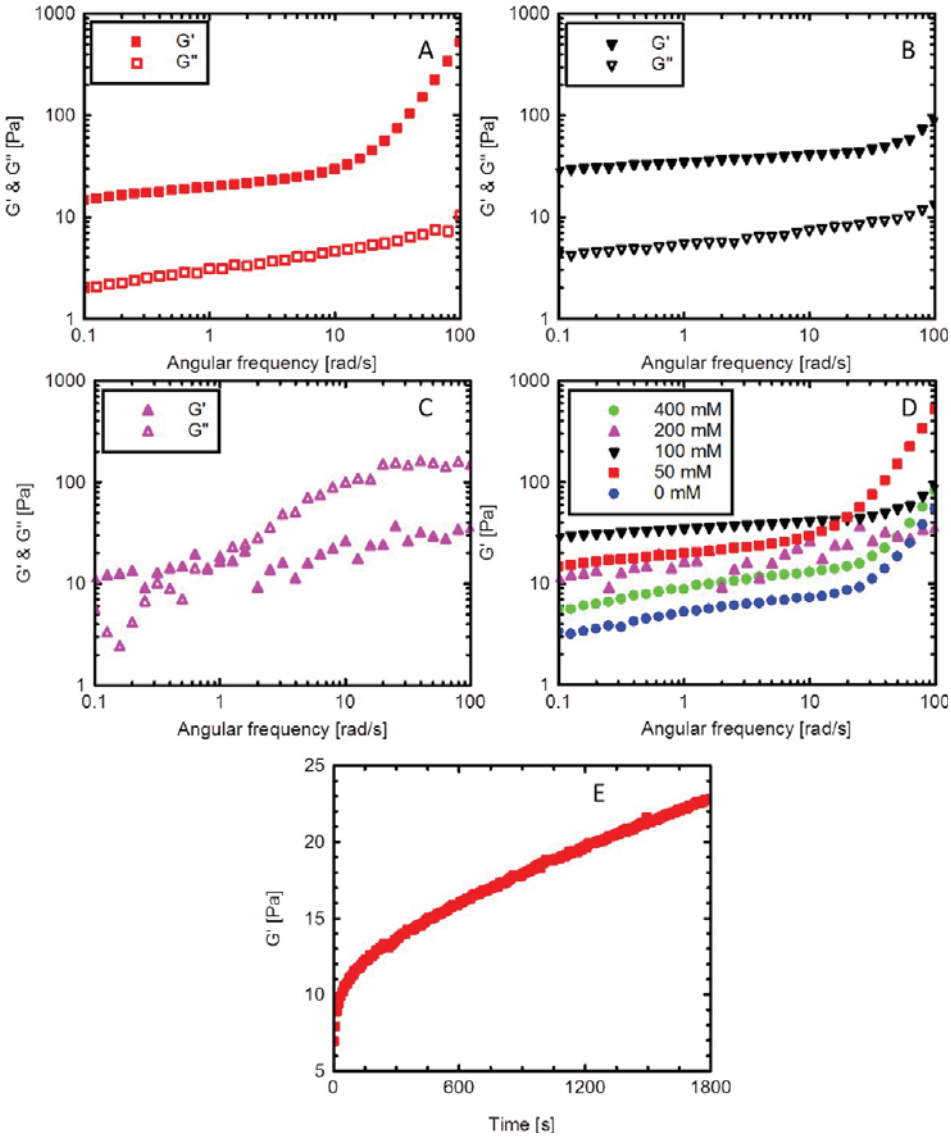

Figure 2. Rheological characterization of 2 wt % β-lactoglobulin protein fibrils at varying ionic strengths: (A) 50 mM, (B) 100 mM, and (C) 200 mM ionic strength. (D) Storage modulus determined at different ionic strengths by frequency sweeps. (E) Structural recovery behavior of the fibril gel prepared at the ionic strength of 50 mM as a function of time after destruction of the gel by a 100% oscillatory shear strain.

Figure 2E shows the structural recovery behavior of the fibril gels as a function of time. The steady-state recovery of the storage modulus clearly demonstrates the self-healing features of the protein gels.

We then move forward in the study of the phase diagram by combining various scattering techniques. We start by following the evolution in the SANS data on increasing concentrations of the protein fibrils. Figure 3 shows the SANS 2D spectra collected at 0.3 and 4 wt % β-lactoglobulin amyloid fibrils and no salt. Figure 3A shows the 2D isotropic scattering profile acquired from the dispersion of 0.3 wt % protein fibrils, that is, still in the isotropic state. Above the isotropic−nematic transition, the SANS 2D pattern becomes highly anisotropic, as shown in Figure 3B, where the 2D scattering profile of the 4 wt % nematic dispersion is shown. The corresponding azimuthal profile is given in Figure 3C, where the two maxima in scattered intensity at 30° and 210° (measured clockwise from the vertical) arise from the alignment of the fibrils along a macroscopic nematic director; accordingly, the same sample in Figure 3B,C placed between cross polarizers shows bright birefringence, confirming the occurrence of the nematic phase.

Further insight into the organization of the protein fibrils and the characteristic length scales upon increase of concentration can be gained by azimuthally averaging the measured scattered intensities at the same scattering angles and plotting the averaged scattered intensity against the scattering vector $q = (4\pi/\lambda)\sin(\theta/2)$, with λ the neutrons wavelength and θ the scattering angle. The data collected at different concentrations are normalized and given in absolute intensities in Figure 3D. The measured scattering intensities, $I(q)$ can be interpreted in terms of $I(q) = N/V(\Delta k)^2 P(q)S(q)$, where N is the number of scatterers contained in the studied volume V, Δk is the difference of scattering lengths between the protein fibrils and the solvent, $P(q)$ is the form factor of protein fibrils, yielding the information about the size and shape of the fibrils, and $S(q)$ is the structure factor related to the mutual interaction and organization of the fibrils in the solution. The protein fibrils are polydispersed in shape and size, so the measured intensities

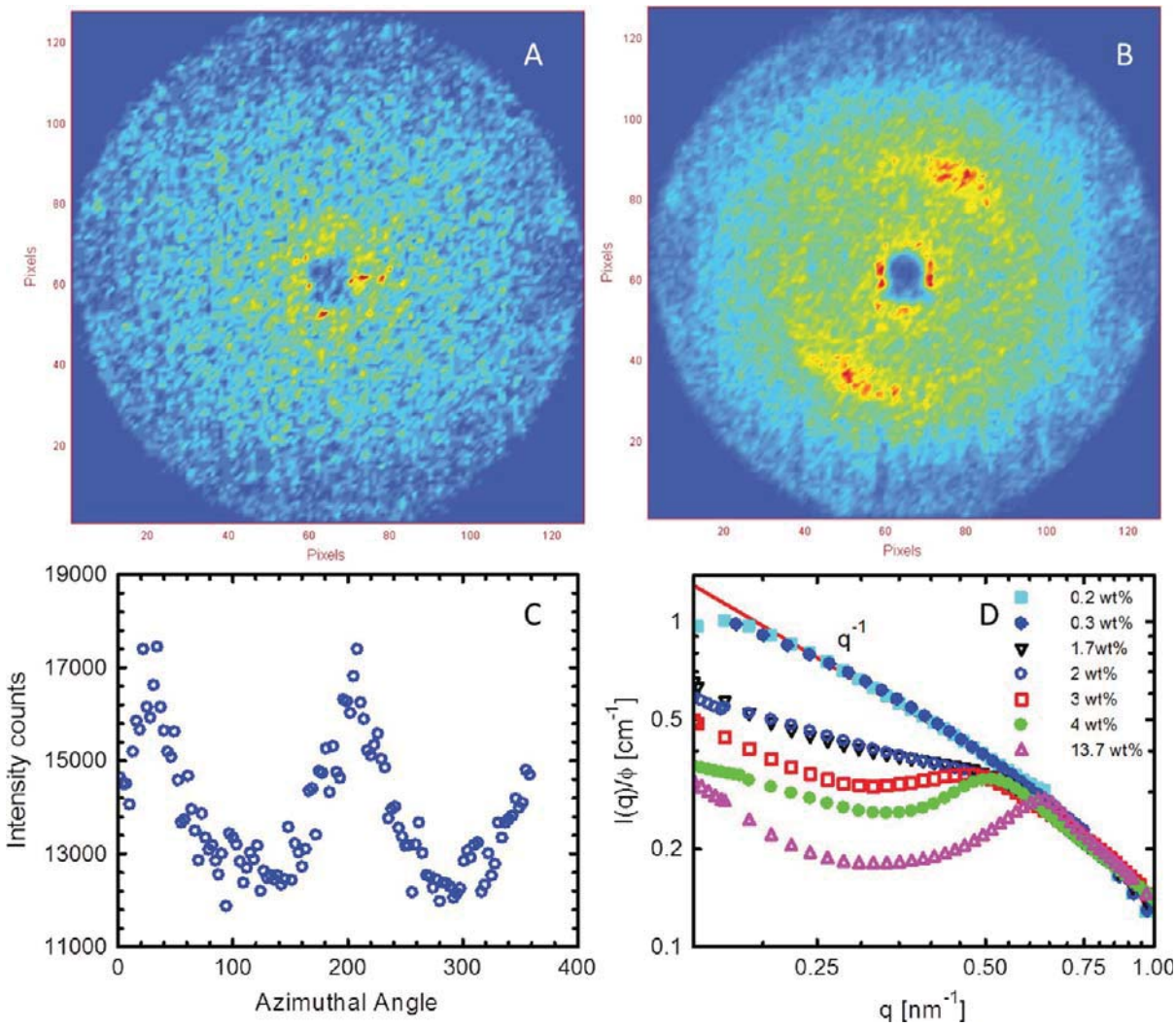

Figure 3. Small angle neutron scattering (SANS) at different concentration of the protein fibrils. (A) 2D SANS diffractogram of a 0.3 wt % β-lactoglobulin fibril suspension in the isotropic phase in (B) the 2D SANS diffractogram is given for a 4 wt % β-lactoglobulin fibril concentration in the nematic phase. (C) Azimuthal intensity evolution of the 2D scattered intensity of the 4 wt % β-lactoglobulin fibril suspension. (D) Normalized scattering intensities measured at the different concentrations of the β-lactoglobulin amyloid fibrils. Upon an increase in concentration, the intensities show the development of structure factor peaks due to the interaction of the fibrils.

directly include the average contribution of the fibrils in solution.

The normalized intensities shown in Figure 3D for the concentrations of 0.2 and 0.3 wt % are nearly indistinguishable since the structure factor influence at this diluted concentration is very close to 1 at any q. In other words, the measured scattered intensities at these low concentrations yield directly the form factor $P(q)$ of the fibrils. At low q, the intensities follow an asymptotic slope of -1, a signature of the rigid rodlike nature of the fibrils in this q region. The detailed discussion of the protein fibrils form factor at different q regions and length scales is available in our earlier reports.[4] A more detailed description of the fibrils form factor capturing their multistranded twisted ribbon structures is also available from earlier reports of our group.[28] Here we are particularly interested with the appearance of the structure factor upon increase in fibrils concentration, as a result of the increasingly strong interactions among protein fibrils. As it can be observed in Figure 3D, at high enough concentrations (1.7 wt %), the normalized intensities show the appearance of a broad characteristic shoulder at 0.48 nm^{-1}. With a further increase of the protein fibril concentrations, the structure factor peak becomes sharper and progressively shifts toward higher q regions, e.g., lower characteristic length scales: from a concentration 3 wt % upward, the peak maximum becomes easily resolvable, and at a concentration of 13.7 wt %, the peak maximum has shifted to a q value of 0.61 nm^{-1}, corresponding to interfibril characteristic distances of ≈10 nm. Because these length scales are directly comparable with the diameter of the fibrils, and considering the highly anisotropic pattern of the azimuthal scattered intensities (see Figure 3C), the structure factor peak in the scattered intensity can be clearly interpreted in terms of the repulsive liquid crystalline interactions among fibrils leading to the formation of a highly structured macroscopic nematic phase: above the isotropic−nematic transition, upon increasing concentrations, the crowding of the protein fibrils in the colloidal dispersion leads to progressively smaller interfibril distances, (comparable with their diameter and approaching the close-packing distance), the increase in the sharpness of the structure factor peak, and a steady increase in the orientation order.

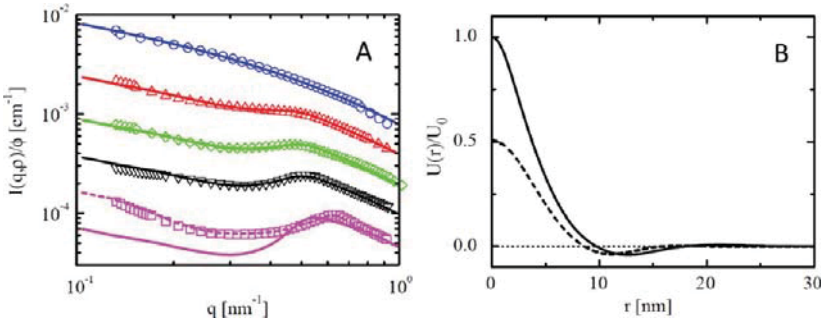

Figure 4. (A) Measured scattering intensity $I(q, \rho)$ of β-lactoglobulin fibrils without added salt for five fibril concentrations: 0.3, 1.7, 3, 4, 13.7 wt % (from top to bottom). For clarity, the lowermost scattering densities have been shifted down by a factor of 2, 4, 8, 16, respectively. The solid lines represent the results of the integral equation theory using the effective interaction potential $U(r)$ shown by the solid line in panel B. The dotted line in panel A displays the calculated results for the highest concentration but using the interaction potential given by the dashed line in panel B. The effective interaction potentials $U(r)$ are normalized such that $U_0 = U(r = 0)$ for the solid line in panel B.

To further rationalize the observed behavior, and in the view of the rather complex experimental system, we use an established theoretical framework allowing the comparison of the measured scattered intensities with the theoretical expected ones.

As anticipated above, SANS determines the scattering intensity $I(q, \rho)$ as a function of the scattering vector q and the particle number density ρ. Within the "Polymer Reference Interaction Site Model" (PRISM), introduced by Schweizer and Curro in 1987,[29] the structure factor for a system consisting of monodisperse interacting particles can be conveniently rewritten as (see also Supporting Information)[30]

$$S(\mathbf{q}, \rho) = 1 + \rho h(\mathbf{q}, \rho)/(P(\mathbf{q})) \quad (1)$$

where ρ is the number particle density. Here we have adopted spherical coordinates for the scattering vector with $|\mathbf{q}|^2 = q^2 = q_z^2 + q_\perp^2$ (where subscript $\perp$ refers to the plane orthogonal to the z-axis). $P(\mathbf{q})$ is, again, the form factor, e.g., a particle-averaged intramolecular correlation function which characterizes the geometric shape of the particles. Hence $P(\mathbf{q})$ describes how the scattering intensity is modulated by interference effects between radiation scattered by different parts of the same particle. For flexible particles, the intramolecular correlation function depends on the particle number density and follows from a statistical average over particle configurations.[31,32] The term $h(\mathbf{q}, \rho)$ is the particle-averaged total correlation function and, together with the particle averaged direct correlation function, $c(\mathbf{q}, \rho)$, used in the Ornstein−Zernike formalism (see below), quantify the structural order of the fluid and are related to mutual interactions between different particles. These correlation functions are calculated numerically by solving the generalized Ornstein−Zernike equation:

$$h(\mathbf{q}, \rho) = P(\mathbf{q})c(\mathbf{q}, \rho)P(\mathbf{q}) + \rho c(\mathbf{q}, \rho)h(\mathbf{q}, \rho)P(\mathbf{q}) \quad (2)$$

together with the Laria−Wu−Chandler closure relation:[33]

$$h(r, \rho) = \ln[h(r, \rho) + 1] + P(r) \\ *[c(r, \rho) + U(r)/(k_BT)]*P(r) \quad (3)$$

for a particle-averaged interaction potential $U(r)$ between two different particles, where the $*$ denotes a convolution product. The Laria−Wu−Chandler closure relation allows determining the interaction potential among particles, $U(r)$, from scattering information, going from the scattering vector domain (q) into the real space domain (r). In the format discussed above, the PRISM integral theorem does not (yet) include anisotropic liquid crystalline interactions, and a justification of such an approximation in treating the experimental SANS data is given in full in the Supporting Information. We anticipate that liquid crystalline interactions can actually be included in the PRISM formalism to account for liquid crystalline order and interactions, and this has been done later in this manuscript when treating static light scattering experiments, in which such a refinement proved to be necessary at those length scales (see the following discussion around Figure 5 and the Supporting Information).

The interaction potential calculated for the present system via eqs 1−3 is shown by the solid line in Figure 4B, and the corresponding calculated scattering intensities are displayed by the solid lines in Figure 4A for five volume fractions $\phi = \rho$Vp = 0.003, 0.017, 0.03, 0.04, 0.137 (from top to bottom), where Vp is the volume of a particle. The dotted line in Figure 4A displays the calculated results for the highest volume fraction ϕ = 0.137 but using the interaction potential given by the dashed line in Figure 4B. The corresponding experimentally determined scattering intensities are shown by the symbols, where the experimental data for ϕ = 0.03, 0.04 and ϕ = 0.137 have been shifted down and up, respectively, in order to allow for a comparison of the shape of the scattering intensities. It is worthwhile to mention that possible concentration-dependent conversion yields of monomers or dimers[34] into fibers are not explicitly taken into account in the calculations. Nevertheless, one may conclude that the interaction potential given by the solid line in Figure 4A together with the PRISM approach according to eqs 1−3 yield shapes of the scattering intensities which are similar to the experimental data for all the volume fractions ϕ in the range [0.003, 0.04]. This interaction potential has to be considered as an effective interaction potential taking into account both the various interactions mentioned in earlier papers on β-lactoglobulin fibrils and many body effects. The generalized Ornstein−Zernike equation approach is not suitable to describe the structure of a network in a gel phase. Therefore, the dashed lines in Figure 4A,B are just shown for comparison.

The β-lactoglobulin protein fibrils system at different concentrations is characterized further using cross correlation light scattering measurements. Cross correlation effectively suppresses the multiple scattering contribution from concentrated turbid samples by performing two simultaneous scattering measurements at the same scattering volume and same scattering vector and extracting only single scattering information common to both.[35] The measurements were

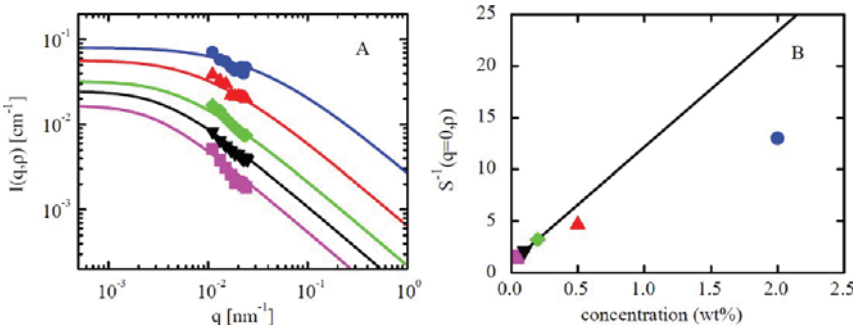

Figure 5. (A) Measured static light scattering intensity $I(q, \rho)$ of β-lactoglobulin amyloid fibrils without added salt for five fibril concentrations: 0.05, 0.1, 0.2, 0.5, 2 wt % (from bottom to top). The solid lines represent the results of the integral equation theory using analytically traceable forms of the intramolecular and direct correlation functions, inclusive of liquid crystalline order. (B) Inverse radially averaged structure factor $S^{-1}(q=0, \rho)$ extrapolated to vanishing scattering vectors for the same five fibril concentrations as in panel A. The solid line represents the result valid for the isotropic phase. The nematic phase overtakes the stability of the isotropic phase when the fibril concentration is predicted to be 0.34 wt % (see the Supporting Information), as found experimentally.

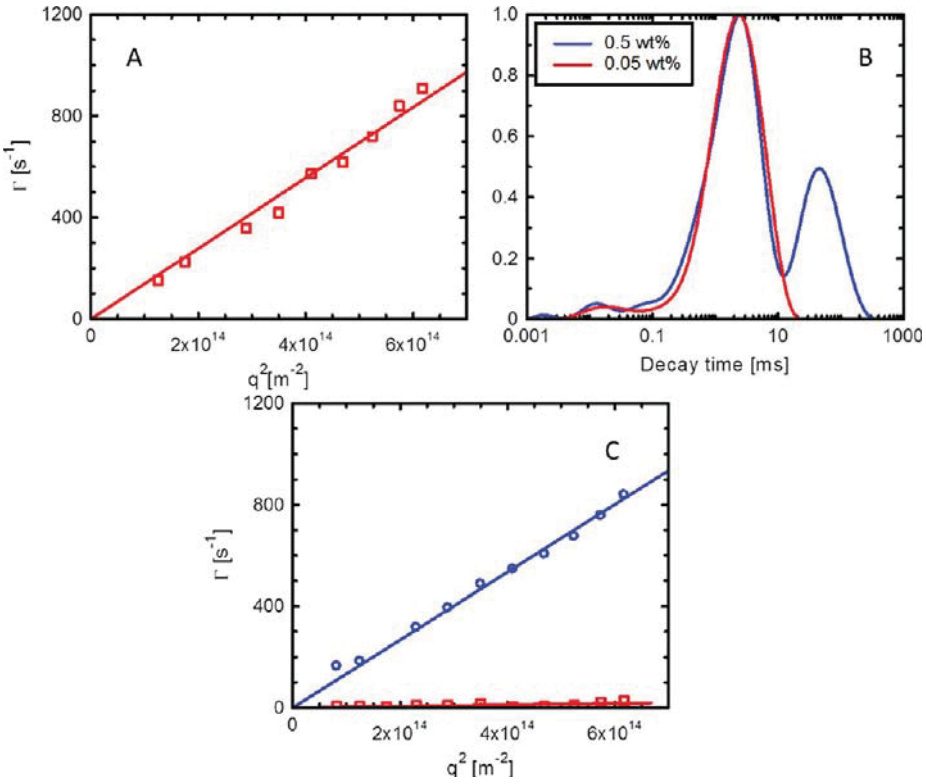

Figure 6. (A) Apparent decay rate of the auto correlation function vs square of the scattering vector at the 0.05 wt % of β-lactoglobulin protein fibrils solution. (B) Apparent relaxation time of the auto correlation function for the 0.05 and 0.5 wt % protein fibrils suspensions measured at 90° scattering angle. (C) Apparent decay rate of the auto correlation function vs square of the scattering vector for the 0.5 wt % β-lactoglobulin protein fibrils system.

performed at different scattering angles to achieve a wide q region. Figure 5A displays SLS intensities of β-lactoglobulin amyloid fibrils without added salt (symbols) together with the calculated radially averaged scattering intensities (lines) using the PRISM model, this time inclusive of the treatment of orientation anisotropic order in the nematic phase, which becomes more relevant at these length scales. Details of the PRISM model adapted to anisotropic systems are provided in the Supporting Information. For the lower three fibril concentrations (0.05 wt %, 0.1 wt %, 0.2 wt %) the isotropic phase is stable, i.e. the usual nematic order parameter $S_2 = 0$ is used, while in the nematic phase $S_2 = 0.7$ and $S_2 = 0.8$ have been used in the calculation for the 0.5 and 2 wt % sample, respectively. The main features of the measured scattering intensities are well captured by the theoretical approach, and two conclusions can be drawn: (a) in the isotropic phase, the q range accessible by SLS is not sufficient to use Guinier's law,[32] $I(q \to 0, \rho \to 0) \sim (1-q^2R_g^2/3)$ in order to determine the radius of gyration R_g in the case of the rather long and stiff β-lactoglobulin amyloid fibrils, thus in the calculations we have used $R_g^2 = L^2/12$ with $L = 2000$ nm, in line with experimental available values;[10] (b) in the nematic phase the experimental determination of thermodynamic properties in the limit of vanishing scattering vectors requires the knowledge of the experimentally not accessible anisotropic form factor $P(\boldsymbol{q})$, which for a semiflexible object may be a function of the nematic

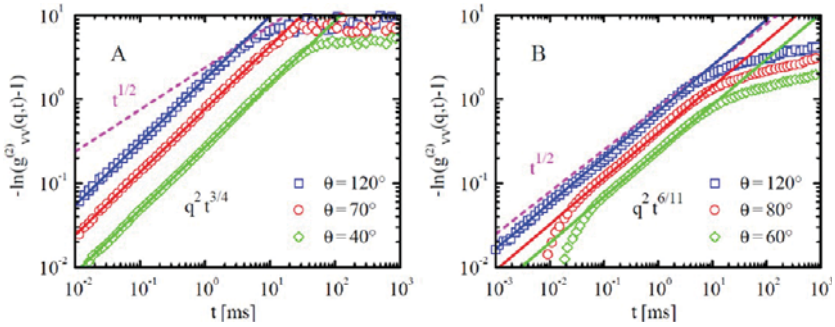

Figure 7. Measured polarized dynamic light scattering intensity autocorrelation function (symbols) of β-lactoglobulin fibrils without added salt in a dilute isotropic solution (0.05 wt %), panel A) and in a semidilute nematic solution (2 wt %), panel B). The solid lines in panel A show the theoretical results as obtained from eqs 4 and 5, which exhibit the $q^2t^{3/4}$ scaling dependence characteristic of bending relaxation modes. The solid lines in panel B demonstrate the $q^2t^{6/11}$ scaling dependence due to the slowed intrafibrillar dynamics; in both panels, the dashed line of slope $t^{1/2}$ representing the time dependence of the Rouse model is given for comparison. In panel B, cooperative motions lead to a weak time dependence for longer times, while translational motion leads to a q^2t scaling dependence for short times and small magnitudes of the scattering vector q.

order parameter and hence also of the particle number density. From the PRISM fit to the static light scattering measurements, we extract the theoretical structure factor (see the Supporting Information) extrapolated to $q = 0$, $[S(q = 0)]$ for all the concentrations investigated. This value is related to the osmotic compressibility $RT(\partial\pi/\partial c)^{-1}$ by the relation:[36] $[S(q=0)] = (RT/M)(\partial\pi/\partial c)^{-1}$ or, which is equivalent, $[S(q=0)] = k_BT(\partial\pi/\partial\rho)^{-1}$, where we have used $\rho=cN_A/M$ to relate the mass concentration c to the number particle density ρ, with M and N_A the molar mass of fibrils and the Avogadro number, respectively. In Figure 5B we give the extrapolated inverse of $S(q=0,\rho)$ values plotted against the concentration of fibrils. The solid line displays the analytic result for the isotropic phase of the inverse averaged structure factor $S^{-1}(q=0, \rho) \approx 1 + 2B_2\rho = 1 + 4Ld_{eff}\phi(9d^2)$, where B_2 is the usual second virial coefficient, d_{eff} is the effective diameter of the fibrils, as derived in refs 22 and 23 and in the Supporting Information, and the other symbols have been defined before. The slope of $S^{-1}(q = 0, \rho)$ with increasing concentration, e.g., B_2, is lowered in the nematic phase (upper two data points) since alignment causes each fibril to occupy a smaller spanned volume, overlapping less with its neighbors. As a consequence, the osmotic pressure $\pi = k_BT \int d\rho\ S^{-1}(q = 0, \rho)$ exhibits in the nematic phase the well-known more gradual increase as a function of concentration as compared to the isotropic phase.[30,37,38]

In addition to the static light scattering experiments on the fibril suspensions, dynamic light scattering measurements were also performed by the modulated cross correlation light scattering technique. Polarized dynamic light scattering allows one to measure the time dependent intensity correlation function $g_{(2)}^{VV}(q, t)$, which is related via the Siegert relation to the scattered electric field correlation function $(g_{(2)}^{VV}(q, t) - 1)^{1/2}$. For a suspension of perfectly rigid noninteracting colloidal objects, the term $(g_{(2)}^{VV}(q, t) - 1)^{1/2}$ is well-known to decay exponentially with the correlation time, yielding the diffusion coefficient via the analysis of the decay rate.

Figure 6 shows the polarized dynamic light scattering results measured at different protein fibril concentrations. The measurements are performed at different scattering angles. The correlation functions are analyzed by the CONTIN method. The apparent decay rate of the autocorrelation function vs square of the scattering vector (q^2) at the protein fibril concentration of 0.05 wt % is shown in Figure 6A. The apparent decay rate is linearly dependent with q^2. The apparent decay rate remains the same with the increase of the protein fibril concentration until 0.3 wt %. However, with the further increase of concentration to 0.5 wt %, the apparent decay rate of the correlation function shows a bimodal distribution. The analysis of the correlation function measured at 0.5 wt % is shown in Figure 6B. The apparent relaxation decay rate shows both a fast and a slow mode, revealing both individual and collective diffusion of the protein fibrils in a denser semidilute nematic phase. The peaks at the lowest decay time are mainly due to the presence of the protein monomers and the protofilaments. The collective and the individual apparent relaxation decay rates at different scattering angles are measured and given in Figure 6C against the q^2. The apparent relaxation decay rate corresponding to the collective translational diffusion is 2 orders of magnitude slower than the relaxation decay rate of the single protein fibrils, which clearly captures the phase transition of the protein fibrils from isotropic to the nematic phase on fibril concentration increase.

In the above analysis, which is a rather simplified approach for such a complex experimental system, we have purposely talked about apparent decay rate because the DLS autocorrelation function was forced to decay exponentially by ignoring more complex features arising from internal motion of the fibrils. Indeed, if the colloidal object diffusing light is nonrigid and characterized by internal motion modes and/or structural changes, the time decay function of $(g_{(2)}^{VV}(q, t) - 1)^{1/2}$ is no longer a perfect exponential. For a dilute solution containing noninteracting wormlike polymers, $g_{(2)}^{VV}(q, t)$ has been shown to obey the stretched exponential function:

$$\sqrt{g_{(2)}^{VV}(q, t) - 1} = \exp(-Aq^2t^{3/4}) \tag{4}$$

with

$$A = \frac{\Gamma(1/4)}{3\pi}\left(\frac{k_BT}{4\pi\eta}\frac{\ln(\Lambda/d)}{l_p^{1/3}}\right)^{3/4} \tag{5}$$

provided that bending modes dominate the internal dynamics.[39−41] Here the temperature T and the viscosity η characterize the solvent, while Λ, d, and l_p are the hydrodynamic screening length, the diameter, and the persistence length, respectively. Moreover, $\Gamma(x)$ is the gamma function. Equation 4 does not depend on the contour length L of the wormlike polymers and is valid for large scattering vectors $q\cdot l_p \geq 1$. The stretched exponential time decay of the time

dependent intensity autocorrelation function with the exponent 3/4 is a characteristic feature of bending relaxation modes.

Figure 7A displays examples of measured and calculated time dependent intensity autocorrelation functions of β-lactoglobulin fibrils (0.05 wt %) without added salt. The stretched exponential function of time is clearly visible in the time interval t $[10^{-2}-10^{1}]$ ms. Moreover, the time dependent intensity autocorrelation function is a universal function of $q^2t^{3/4}$ on this time scale. However, one cannot extract the model parameters Λ, d, and l_p individually according to eqs 4 and 5. In principle, one could extract the diameter d from the so-called initial decay rate of the time dependent intensity autocorrelation function for times shorter than the ones considered in Figure 7A.[41] However, for the β-lactoglobulin fibrils under consideration there are additional contributions to the measured time dependent intensity autocorrelation functions from free monomers for short times, which do not allow a precise determination of d from the experimental data. However, using the value d = 5.76 nm previously determined by SANS[28] together with l_p = 1620 nm, which is the persistence length for the most frequently observed population of multistranded β-lactoglobulin twisted ribbons, (n = 2),[10] yields Λ = 50 nm from a comparison of the calculated (lines) and measured (symbols) time dependent autocorrelation functions shown in Figure 7A. The screening length Λ accounts for the hydrodynamic screening effects by the surrounding fibrils. For comparison, we note that the stretched exponential function given by eq 4 has been observed experimentally for actin filaments[42,43] and fibrin fibrils[44] in the same time interval. These wormlike biopolymers are both thicker and stiffer than the β-lactoglobulin fibrils under consideration.

The time dependent electric field autocorrelation functions shown in Figure 7A exhibit a rapid relaxation for short times t_{cr} $\leq$ 40 ms, which changes into a plateau for longer times. This plateau arises from restricted transverse fluctuations as discussed in more details elsewhere.[45] These transverse fluctuations are of particular importance for wormlike biopolymers because internal longitudinal fluctuations are suppressed by the constraint of inextensibility. The dynamics of such wormlike biopolymers is often characterized by their mean transverse square displacement $\Delta r_\perp^2(t)$, which is a measure for the average distance a subunit moves perpendicular to the polymer within the time period t. In order to determine the mean transverse square displacement, as a first approximation one may use the relation[46]

$$\sqrt{g_{(2)}^{VV}(q,t) - 1} = \exp(-q^2\Delta r_\perp^2(t)/4) \tag{6}$$

For the β-lactoglobulin fibrils under consideration, the crossover time t_{cr} to the plateau value of the time dependent intensity autocorrelation functions leads to $\Delta r_\perp^2(t_{cr}) \approx$ 80 nm as a measure of the maximum transverse displacement due to bending motion. On longer times scales, these bending modes are already equilibrated for the case of the dilute β-lactoglobulin solution considered in Figure 7A. In contrast to the dynamics in the dilute isotropic solution, Figure 7B shows that the time dependent autocorrelation functions of β-lactoglobulin fibrils in the semidilute nematic solution (2 wt %) exhibit a weak time dependence for times longer than the aforementioned crossover time t_{cr}. Such a weak time dependence has also been observed for fibrin networks[44] and implies that there are a few cooperative motions of fibrils that dissipate energy for times longer than about 10 ms. For comparison, we note that this slow dynamics also leads to the low-frequency dependence of the shear modulus for small frequencies. While the time dependent autocorrelation function exhibits the $q^2t^{3/4}$ scaling dependence due to bending relaxation modes in the dilute solution (Figure 7A), the scaling variable $q^2t^{6/11}$ (see e.g., refs 46−48 and references therein) is found for the 2 wt % fibril semidilute nematic solution (solid lines in Figure 7B). The corresponding intrafibrillar dynamics dominates motion on an intermediate time scale. For times longer than a crossover time $t_{cr} \approx$ 5 ms, the intrafibrillar dynamics is restricted by the surrounding fibrils. Of course, the mean maximum transverse displacement $\Delta r_\perp^2(t_{cr}) \approx$ 20 nm is smaller for the semidilute solution (Figure 7B) as compared to the dilute solution (Figure 7A) as is apparent from the different values of the function $-\ln(g_{(2)}^{VV}(q,t) - 1)$ at the crossover times where the experimental data start to deviate from the solid lines. Increasing the concentration reduces the free volume available for intrafibrillar dynamics. For short times and small scattering vectors, one observes translation motion of the fibrils (lower two data sets in Figure 7B) leading to a q^2t scaling dependence of the time dependent intensity autocorrelation function. The corresponding translational diffusion coefficient $D = 3 \times 10^{-12}$ m^2/s characterizes mainly the diffusion parallel to the fibril axis in the crowded environment. For comparison, in parts A and B of Figure 7, we also plot the dashed lines of slope $t^{1/2}$ corresponding to the Rouse dynamics (see, e.g., ref 49 and references therein).

In addition to the polarized dynamic light scattering, we also performed depolarized dynamic light scattering measurements. As the protein fibrils are anisotropic in shape, upon irradiation with the polarized electric field of the incident laser beam, the oscillating Maxwell dipole associated with their shape will have a component orthogonal to the incident polarization plane. This will result in a measurable intensity on a detector with a polarizer oriented orthogonal to the incident electric field, resulting in the depolarized scattering intensity. We measured the depolarized dynamic scattering intensity at different scattering angles for the β-lactoglobulin fibrils at various concentrations. The relaxation decay time of the anisotropic depolarized dynamic light scattering electric field correlation function, $g_1^{VH}(q,t)$, contains both the translational diffusion coefficient (D) and the rotational diffusion coefficient (Θ). For a system composed of rigid anisotropic scatterers, this results in

$$g_1^{VH}(q,t) \approx \frac{1}{15}\langle N\rangle \alpha_{aniso}^{\ 2}\, e^{-(q^2D+6\Theta)t} \tag{7}$$

where $g_1^{VH}(q,t) = (g_2^{VH}(q,t) - 1)^{1/2}$, α_{aniso} is a prefactor accounting for the molecular optical anisotropic part of the polarization tensor, $\langle N\rangle$ is the average number of particles contained in the scattering volume, and the indexes V and H stand for incoming vertically polarized light and measured horizontally polarized light, respectively. The translational diffusion coefficient D and rotational diffusion coefficient Θ are extracted by plotting the decay rate $\Gamma_{VH} = q^2D + 6\Theta$ versus q^2, where the slope corresponds to the translational diffusion coefficient and the intercept equals 6 times the rotational diffusion coefficient.

As a theory of depolarized dynamic light scattering of such a complex system as the one considered here, capable to capture the bending motion of the semiflexible fibrils and their concentration-dependence is not yet available, we treat, to a first approximation, fibrils as rigid systems, and we extract the apparent translational and rotational diffusion coefficients by

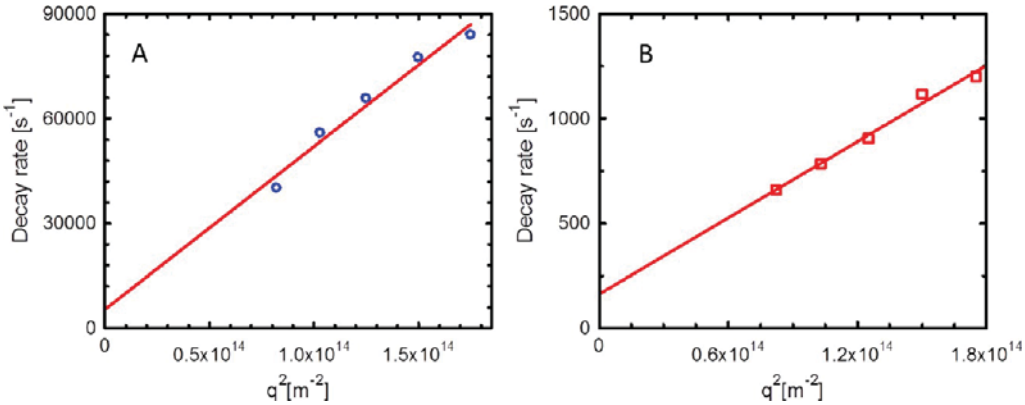

Figure 8. (A) Apparent decay rate of the auto correlation function of the depolarized dynamic light scattering vs the square of the scattering vector at 0.05 wt % β-lactoglobulin protein fibrils concentration. (B) Decay rate vs square of the scattering vector at 0.5 wt % β-lactoglobulin protein fibrils concentration.

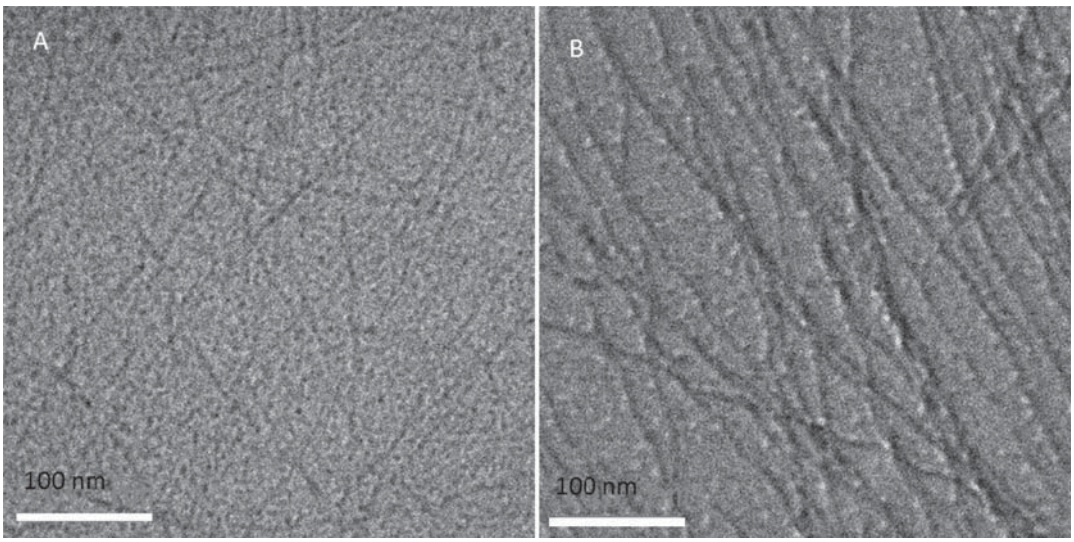

Figure 9. Cryo-TEM representative images of β-lactoglobulin protein fibrils at different concentrations: (A) 0.1 wt % and (B) 0.5 wt % β-lactoglobulin fibrils. The 2D alignment of the protein fibrils along a common direction becomes visible at concentrations beyond the isotropic–nematic transition threshold.

ignoring internal motion modes of the fibrils. The apparent decay rate at different scattering angles is calculated by CONTIN analysis. Figure 8A shows the apparent decay rate vs q^2 at 0.05 wt % protein fibrils concentration, and the rotational diffusion coefficient Θ calculated from the intercept is 895 s^{-1}. The rotational coefficient remains nearly unchanged in the isotropic state, indicating free rotation of the fibrils (see the Supporting Information, Table S1). As the concentration of the protein fibril increases above 0.4 wt %, the depolarized dynamic light scattering relaxation shows an additional relaxation rate as shown in Figure 8B, corresponding to a rotational diffusion coefficient of 27 s^{-1} (the faster motion apparent relaxation time is not shown in Figure 8B due to the large change in the vertical axis scale but is identical to the one analyzed in Figure 8A). This additional slow decay rate is likely to be due to the hindered rotational diffusion of the protein fibrils in the nematic phase. These results are further, additional evidence that changes in orientation order from the isotropic to the nematic phase can be investigated through the changes in rotational diffusive behavior as revealed by depolarized dynamic light scattering.

To further assess the orientation order directly in real space, the protein fibrils at different concentrations were studied by cryo-TEM. Figure 9 shows the β-lactoglobulin protein fibrils at 0.1 and 0.5 wt % concentration. Cryo-TEM imaging is virtually exempt from introducing artifacts during the sample preparation procedure, such as substrate effects, solvent evaporation during drying, or changes in interactions due to chemical staining to enhance the contrast to the electron beam. However, it only offers a 2D projection of the colloidal dispersion, and in the present case, the presence of long semiflexible objects confined within a 100–200 nm thick vitrified water layer induce a 2D confinement of the fibrils. Thus, an average 2D order parameter $\langle S \rangle = \langle 2 \cos^2 \theta - 1 \rangle$ is necessary to quantify the order, where θ is the angle between the individual protein fibrils and the director vector of the global fibril orientation. Figure 9A shows first the cryo-TEM image at 0.1 wt % β-lactoglobulin fibril concentration in the isotropic state. The fibrils are randomly distributed without any apparent alignment, and indeed, the order parameter S is calculated to be 0.08. Figure 9B shows a representative cryo-TEM image at 0.5 wt % β-lactoglobulin protein fibrils concentration, e.g., in the nematic phase. Here, the presence

of a global orientation of the fibrils is clearly visible, and the corresponding 2D order parameter is calculated to be of the order of 0.74, which indicates a very good orientation of the fibrils in this regime. Additional cryo-TEM images are given in the Supporting Information, Figure S4.

CONCLUSIONS

We have studied the complex phase behavior and dynamics of multistranded β-lactoglobulin protein fibrils at various ionic strengths and concentrations by combining an unprecedented set of scattering, rheological, and microscopy techniques, and we have supported our experimental study by theoretical calculations based on the integral equation theory and the bending relaxation modes to assess the thermodynamic and dynamic behavior, respectively. Depending on the region of the phase diagram, the β-lactoglobulin fibrils can undergo both an isotropic−nematic and a sol−gel phase transition with the increase in fibril concentration (at constant ionic strength) or with an increase in ionic strength (at constant concentration). Rheological measurements reveal that the ionic strength has a strong impact on the strength of the gel, which also exhibit self-recovery features after rupturing. The fibrils at different concentrations and ionic strengths are then analyzed using small angle neutron scattering, static light scattering, and polarized and depolarized dynamic light scattering. Form factor, structure factor, interaction potential, and osmotic compressibility are extracted from the static neutron and light scattering experiments. All these techniques are capable to capture the thermodynamic features of the isotropic−nematic transition at concentrations of the order of 0.3−0.5 wt %, depending on the ionic strength and experimental technique considered. The individual and cumulative translational and rotational diffusion of the fibrils as well as their self-bending motion, observed by polarized and depolarized light scattering in proximity of the isotropic−nematic transition, also reveal a change in the complex dynamic behavior in the two phases. Finally, the change in the alignment of the fibrils is also studied in real space by use of cryo-TEM and quantified by an order parameter, capturing again the features of the isotropic−nematic transition. This work sheds further light on the complex phase and dynamic behavior of this fascinating biological colloidal system and opens for new directions in the detection possibilities of phase transitions in anisotropic complex fluids.

ASSOCIATED CONTENT

Supporting Information

AFM height images, cryo-TEM images, SANS and SLS data, and PRISM formalism theory. This material is available free of charge via the Internet at http://pubs.acs.org.

AUTHOR INFORMATION

Corresponding Author

*E-mail: raffaele.mezzenga@hest.ethz.ch. Phone: +41 44 632 9140.

Notes

The authors declare no competing financial interest.

ACKNOWLEDGMENTS

The authors gratefully acknowledge Dr. Jozef Adamcik (ETH, Zurich) and Jijo Joy Vallooran (ETH, Zurich) for assistance with experiments and valuable discussions. The authors acknowledge support by Stephan Handschin and the Electron Microscopy Center of ETH Zurich (EMEZ). The authors also acknowledge Dr. Sandor Balog and Dr. Urs Gasser (SANS II, PSI, Villigen) for assistance during the neutron scattering experiments.

REFERENCES

(1) Kontopidis, G.; Holt, C.; Sawyer, L. *J. Dairy Sci.* **2004**, *87*, 785−796.
(2) McKenzie, H. A.; Sawyer, W. H.; Smith, M. B. *Biochim. Biophys. Acta* **1967**, *147*, 73−92.
(3) Panick, G.; Malessa, R.; Winter, R. *Biochemistry* **1999**, *38*, 6512−6519.
(4) Jung, J.-M.; Savin, G.; Pouzot, M.; Schmitt, C.; Mezzenga, R. *Biomacromolecules* **2008**, *9*, 2477−2486.
(5) Bromley, E. H.; Krebs, M. R. H.; Donald, A. M. *Faraday Discuss.* **2005**, *128*, 13−27.
(6) Hoffmann, M. A.; van Mil, P. J. *J. Agric. Food Chem.* **1999**, *47*, 1898−1905.
(7) Mehalebi, S.; Nicolai, T.; Durand, D. *Int. J. Biol. Macromol.* **2008**, *43*, 129−135.
(8) Gosal, W. S.; Clark, A. H.; Ross-Murphy, S. B. *Biomacromolecules* **2004**, *5*, 2408−2419.
(9) Loveday, S. M.; Wang, X. L.; Rao, M. A.; Anema, S. G.; Singh, H. *J. Agric. Food Chem.* **2011**, *59*, 8467−8474.
(10) Adamcik, J.; Jung, J.-M.; Flakowski, J.; Rios, P. D. L.; Dietler, G.; Mezzenga, R. *Nat. Nanotechnol.* **2010**, *5*, 423−428.
(11) Bolisetty, S.; Adamcik, J.; Mezzenga, R. *Soft Matter* **2011**, *7*, 493−499.
(12) Kuhn, K. R.; Cavallieri, A. L. F; Da Cunha, R. L. *Int. J. Food Sci. Technol.* **2010**, *45*, 348−357.
(13) Gosal, W. S.; Clark, A. H.; Pudney, P. D. A.; Ross-Murphy, S. B. *Langmuir* **2002**, *18*, 7174−7181.
(14) Hongsprabhas, P.; Barbut, S. *Food Res. Int.* **1996**, *29*, 135−139.
(15) Mulvihill, D. M.; Kinsella, J. E. *J. Food Sci.* **1988**, *53*, 231−236.
(16) Ako, K.; Nicolai, T.; Durand, D. *Biomacromolecules* **2010**, *11*, 864−871.
(17) Nicolai, T.; Britten, M.; Schmitt, C. *Food Hydrocolloids* **2011**, *25*, 1945−1962.
(18) Veerman, C.; Baptist, H.; Sagis, L. M.; van der Linden, E. *J. Agric. Food Chem.* **2003**, *51*, 3880−3885.
(19) Adamcik, J.; Mezzenga, R. *Soft Matter* **2011**, *7*, 5437−5443.
(20) Hamley, I. W. *Soft Matter* **2010**, *6*, 1863−1871.
(21) Sagis, L. M. C.; Veerman, C.; van der Linden, E. *Langmuir* **2004**, *20*, 924−927.
(22) Jung, J.-M.; Mezzenga, R. *Langmuir* **2010**, *26*, 504−514.
(23) Mezzenga, R.; Jung, J.-M.; Adamcik, J. *Langmuir* **2010**, *26*, 10401−10405.
(24) Müller, C.; Inganäs, O. *J. Mater. Sci.* **2011**, *46*, 3687−3692.
(25) Corrigan, A. M.; Muller, C.; Krebs, M. R. H. *J. Am. Chem. Soc.* **2006**, *128*, 14740−14741.
(26) Bolisetty, S.; Hoffmann, M.; Lekkala, S.; Hellweg, Th.; Ballauff, M.; Harnau, L. *Macromolecules* **2009**, *42*, 1264−1269.
(27) Adamcik, J.; Mezzenga, R. *Macromolecules* **2012**, *45*, 1137−1150.
(28) Jones, O. G.; Handschin, S.; Adamcik, J.; Harnau, L.; Bolisetty, S.; Mezzenga, R. *Biomacromolecules* **2011**, *12*, 3056−3065.
(29) Schweizer, K. S.; Curro, J. G. *Phys. Rev. Lett.* **1987**, *58*, 246−249.
(30) Harnau, L. *Mol. Phys.* **2008**, *106*, 1975−2000.
(31) Bolisetty, S.; Airaud, C.; Xu, Y.; Müller, A. H. E.; Harnau, L.; Rosenfeldt, S.; Lindner, P.; Ballauff, M. *Phys. Rev. E* **2007**, *75*, 040803.
(32) Bolisetty, S.; Rosenfeldt, S.; Rochette, C.; Harnau, L.; Lindner, P.; Xu, Y.; Müller, A.; Ballauff, M. *Colloid Polym. Sci.* **2009**, *287*, 129−138.
(33) Laria, D.; Wu, D.; Chandler, D. *J. Chem. Phys.* **1991**, *95*, 4444−4453.
(34) Aymard, P.; Durand, D.; Nicolai, T. *Int. J. Biol. Macromol.* **1996**, *19*, 213−221.

(35) Pusey, P. N. *Curr. Opin. Colloid Interface Sci.* **1999**, *4*, 177−185.
(36) Richtering, W. H.; Schätzle, J.; Adams, J.; Burchard, W. *Colloid Polym. Sci.* **1989**, *267*, 568−576.
(37) Pickett, G. T.; Schweizer, K. S. *J. Chem. Phys.* **2000**, *112*, 4881−4892.
(38) Harnau, L.; Costa, D.; Hansen, J.-P. *EPL* **2001**, *53*, 729−734.
(39) Harnau, L.; Winkler, R. G.; Reineker, P. *J. Chem. Phys.* **1996**, *104*, 6355−6368.
(40) Kroy, K.; Frey, E. *Phys. Rev. E* **1997**, *55*, 3092−3101.
(41) Winkler, R. G.; Harnau, L.; Reineker, P. *Macromol. Theory Simul.* **1997**, *6*, 1007−1035.
(42) Farge, E.; Maggs, A. C. *Macromolecules* **1993**, *26*, 5041−5044.
(43) Gotter, R.; Kroy, E.; Frey, E.; Barmann, M.; Sackmann, E. *Macromolecules* **1996**, *29*, 30−36.
(44) Arcovito, G.; Bassi, F. A.; Spirito, M. D.; Stasio, E. D.; Sabetta, M. *Biophys. Chem.* **1997**, *67*, 287−292.
(45) Harnau, L.; Reineker, P. *Phys. Rev. E* **1999**, *60*, 4671−4676.
(46) Kremer, K.; Binder, K. *J. Chem. Phys.* **1984**, *81*, 6381−6394.
(47) Paul, W.; Binder, K.; Heermann, D. W; Kremer, K. *J. Phys. II (France)* **1991**, *1*, 37−60.
(48) Zettl, U.; Hoffmann, S. T.; Koberling, F.; Krausch, G.; Enderlein, J.; Harnau, L.; Ballauff, M. *Macromolecules* **2009**, *42*, 9537−9547.
(49) Doi, M.; Edwards, S. *The Theory of Polymer Dynamics*; Clarendon Press: Oxford, U.K., 1986.